Human HOIP and LUBAC deficiency underlies autoinflammation, immunodeficiency, amylopectinosis, and lymphangiectasia

Bertrand Boisson,[1]* Emmanuel Laplantine,[2]* Kerry Dobbs,[3] Aurélie Cobat,[6,9] Nadine Tarantino,[2] Melissa Hazen,[3] Hart G.W. Lidov,[4] Gregory Hopkins,[5] Likun Du,[3] Aziz Belkadi,[6,9] Maya Chrabieh,[6,9] Yuval Itan,[1] Capucine Picard,[1,6,7,9] Jean-Christophe Fournet,[9] Hermann Eibel,[10] Erdyni Tsitsikov,[3] Sung-Yun Pai,[5] Laurent Abel,[1,6,9] Waleed Al-Herz,[11,12]** Jean-Laurent Casanova,[1,6,8,9,13]** Alain Israel,[2]** and Luigi D. Notarangelo[3,14]**

[1]St. Giles Laboratory of Human Genetics of Infectious Diseases, Rockefeller Branch, Rockefeller University, New York, NY 10065
[2]Laboratory of Signaling and Pathogenesis, Centre National de la Recherche Scientifique, UMR 3691, Institut Pasteur, 75724 Paris, France
[3]Division of Immunology and The Manton Center for Orphan Disease Research, [4]Department of Pathology, [5]Division of Hematology-Oncology, Boston Children's Hospital, Harvard Medical School, Boston, MA 02115
[6]Laboratory of Human Genetics of Infectious Diseases, Necker Branch, Institut National de la Santé et de la Recherche Médicale UMR1163; [7]Study Center of Immunodeficiencies, APHP; [8]Pediatric Hematology-Immunology Unit, Necker Hospital for Sick Children, 75015 Paris, France
[9]Paris Descartes University, Imagine Institute, 75015 Paris, France
[10]University Medical Centre Freiburg, Centre of Chronic Immunodeficiency, 79098 Freiburg, Germany
[11]Allergy and Clinical Immunology Unit, Department of Pediatrics, Al-Sabah Hospital, 70459 Kuwait City, Kuwait
[12]Department of Pediatrics, Kuwait University, 13110 Kuwait City, Kuwait
[13]Howard Hughes Medical Institute, New York, NY 10065
[14]Harvard Stem Cell Institute, Harvard University, Boston, MA 02115

Inherited, complete deficiency of human HOIL-1, a component of the linear ubiquitination chain assembly complex (LUBAC), underlies autoinflammation, infections, and amylopectinosis. We report the clinical description and molecular analysis of a novel inherited disorder of the human LUBAC complex. A patient with multiorgan autoinflammation, combined immunodeficiency, subclinical amylopectinosis, and systemic lymphangiectasia, is homozygous for a mutation in *HOIP*, the gene encoding the catalytic component of LUBAC. The missense allele (L72P, in the PUB domain) is at least severely hypomorphic, as it impairs HOIP expression and destabilizes the whole LUBAC complex. Linear ubiquitination and NF-κB activation are impaired in the patient's fibroblasts stimulated by IL-1β or TNF. In contrast, the patient's monocytes respond to IL-1β more vigorously than control monocytes. However, the activation and differentiation of the patient's B cells are impaired in response to CD40 engagement. These cellular and clinical phenotypes largely overlap those of HOIL-1–deficient patients. Clinical differences between HOIL-1– and HOIP-mutated patients may result from differences between the mutations, the loci, or other factors. Our findings show that human HOIP is essential for the assembly and function of LUBAC and for various processes governing inflammation and immunity in both hematopoietic and nonhematopoietic cells.

CORRESPONDENCE
Jean-Laurent Casanova: casanova@rockefeller.edu
OR
Luigi D. Notarangelo: luigi.notarangelo@childrens.harvard.edu

Abbreviations used: EDA-ID, ectodermal dysplasia with immunodeficiency; LUBAC, linear ubiquitination chain assembly complex; SNP, single-nucleotide polymorphism.

*B. Boisson and E. Laplantine contributed equally to this paper.
**W. Al-Herz, J.-L. Casanova, A. Israel, and L.D. Notarangelo contributed equally to this paper.

The Rockefeller University Press $30.00
J. Exp. Med. 2015 Vol. 212 No. 6 939–951
www.jem.org/cgi/doi/10.1084/jem.20141130

The description and analysis of inborn errors of human NF-κB–mediated immunity began in 2001 with the discovery of X-linked recessive anhidrotic ectodermal dysplasia with immunodeficiency (EDA-ID) caused by hypomorphic mutations in *NEMO* (encoding NF-κB essential modulator; Döffinger et al., 2001), followed by the description of autosomal dominant EDA-ID caused by hypermorphic mutations of the *NFKBIA* gene (encoding IκBα) in 2003 (Courtois et al., 2003). These defects lead to a broad range of infections, caused by impaired signaling by various membrane receptors involved in innate and adaptive immunity, including TLR/IL1R and TNFRs (Puel et al., 2004; Casanova et al., 2011; Picard et al., 2011; Boisson et al., 2015). Gain-of-function mutations of IκBα are also associated with a profound T cell deficiency (Courtois et al., 2003). Other global defects of NF-κB activation were later discovered, including autosomal recessive IKKβ deficiency (Pannicke et al., 2013; Mousallem et al., 2014; Nielsen et al., 2014) in the canonical pathway and autosomal-dominant NFKB2 deficiency (Lee et al., 2014; Lindsley et al., 2014) and autosomal recessive NIK deficiency (Willmann et al., 2014) in the alternative pathway.

There are many more inborn errors of specific pathways involving NF-κB caused by mutations in receptors or their ligands, such as CD40 (Ferrari et al., 2001) and CD40L (Allen et al., 1993; DiSanto et al., 1993) deficiency. Mutations may also affect cytosolic components, as illustrated by defects of TLR/IL-1-dependent NF-κB–mediated immunity in patients with autosomal recessive IRAK-4 and MyD88 deficiencies (Picard et al., 2003; von Bernuth et al., 2008; Picard et al., 2010; Casanova et al., 2011; Alsina et al., 2014). Patients with these two deficiencies are prone to life-threatening pyogenic bacterial diseases (Picard et al., 2010). In these inborn errors of immunity, signs of inflammation during infection are either absent or delayed (Picard et al., 2011). Collectively, these experiments of nature highlight the diversity of cells and receptors that engage NF-κB activation. They provide some explanation for some of the clinical phenotypes seen in patients with inborn errors of core NF-κB components. However, most of these receptors can normally also engage other signaling pathways, somewhat blurring some of the latter clinical phenotypes.

Surprisingly, bi-allelic mutations of *HOIL1*, encoding one of the three proteins of the linear ubiquitination chain assembly complex (LUBAC), a component of the NF-κB cascade involved in IKK complex activation (Iwai and Tokunaga, 2009; Tokunaga et al., 2009; Fujita et al., 2014; Popovic et al., 2014), were recently shown to underlie autoinflammation, immunodeficiency, and amylopectinosis (Boisson et al., 2012). The assembly of LUBAC was impaired but its function was not tested. The fibroblasts of HOIL-1–deficient patients display impaired responses to TLR agonists, IL-1β, and TNF, and their B cells display an impaired response to CD40L. In contrast, monocytes from these patients respond more strongly than control monocytes to IL-1β (Boisson et al., 2012). Similar findings were recently documented in a mouse model (MacDuff et al., 2015). We report here a patient with diffuse autoinflammation, combined immunodeficiency, infections, subclinical amylopectinosis, and systemic lymphangiectasia due to a homozygous missense mutation of *HOIP* (*RNF31*), encoding the catalytic component of LUBAC.

RESULTS

Identification of a homozygous *HOIP* missense mutation

We investigated a patient born to consanguineous parents of Kuwaiti descent, who presented with multiorgan autoinflammation, systemic lymphangiectasia, weakness at lower extremities, subclinical amylopectinosis, and a combined immunodeficiency manifesting as chronic diarrhea and recurrent viral and bacterial infections, associated with lymphopenia, antibody deficiency and an impaired distribution and function of T lymphocytes (see case report and Table S1). Periodic Acid-Schiff staining of sternocleidomastoid muscular biopsy showed patches of granular or subsarcolemmal PAS-positive material that was resistant to treatment with diastase, consistent with amylopectinosis, but there were no clinical, electrographic, or echographic signs of skeletal myopathy or cardiomyopathy (Fig. 1 A). We set out to decipher the underlying genetic defect by genome-wide linkage (GWL) and whole-exome sequencing (WES; Bolze et al., 2010; Byun et al., 2010; Itan et al., 2013; Casanova et al., 2014; Conley and Casanova, 2014). We did not find rare variants in known autoinflammation and immunodeficiency genes (Al-Herz et al., 2014; Conley and Casanova, 2014) and in known lymphangiectasia-causing genes (*CCBE1*, *FOXC2*, *VEGFR3*, *SOX18,* and *GJC2*; Alitalo, 2011). We hypothesized that this novel, rare condition would follow an autosomal recessive inheritance. We therefore filtered out all heterozygous and common variant. We found 38 homozygous rare variants in as many genes (minor allele frequency ≤1%; Table S2). GWL by homozygosity mapping with a model of complete penetrance further reduced the list of variations to 15 candidate genes (Table S2). These variants included a homozygous T-to-C substitution at position 215 (c.215T>C) in exon 2 of *HOIP* (also known as *RNF31*), which was identified in the patient and confirmed by Sanger sequencing (Fig. 1, B and C). This missense substitution results in the replacement of a leucine residue by a proline residue at the start of the PUB (PNGase [peptide N-glycosidase]/ubiquitin-associated) domain of HOIP (Fig. 1 D). Both parents and the healthy sibling of the patient were heterozygous for the mutation (Fig. 1, B and C). The HOIP L72P variant was not found in public databases (NCBI, UCSC, 1000 genomes, or ExAC, reaching a total of up to 60,706 individuals) or in our own WES database (2,212 individuals). Possibly relevant to the patient's clinical phenotype, *HOIP* encodes HOIL-1–interacting protein, the catalytic components of LUBAC, an E3 ligase complex (Fig. 1 D) responsible for adding head-to-tail linear polyubiquitin chains to substrate proteins, including NEMO (Kirisako et al., 2006; Iwai and Tokunaga, 2009; Tokunaga et al., 2009; Smit et al., 2012; Sasaki et al., 2013), RIP1 (Gerlach et al., 2011), and ASC (Boisson and Casanova, 2014; Rodgers et al., 2014). No rare mutations were found

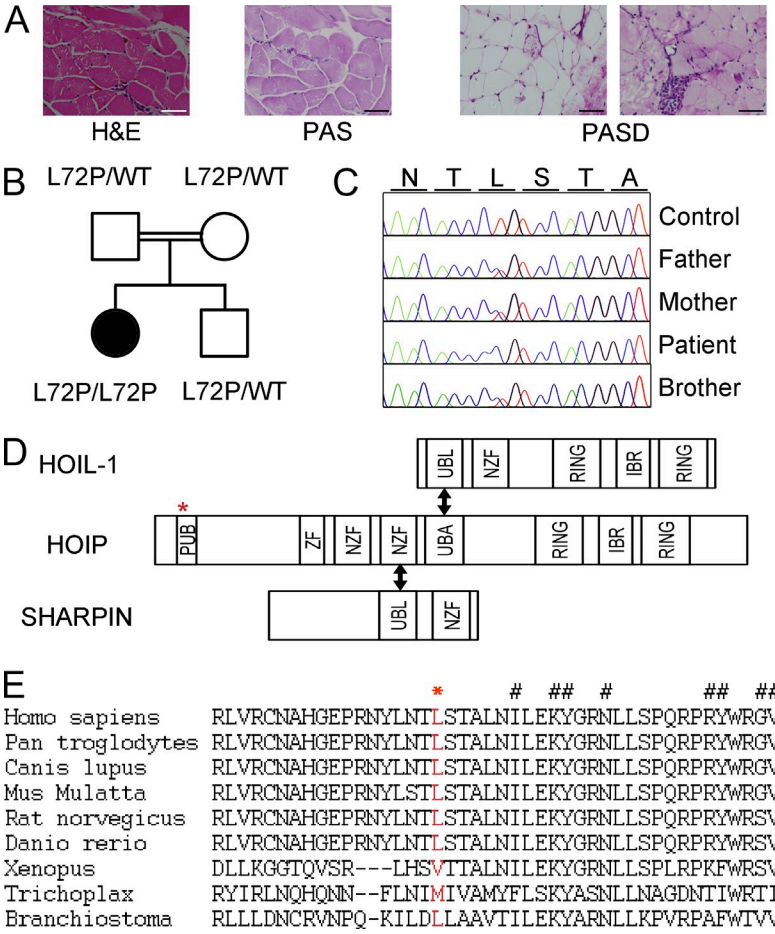

Figure 1. A patient with a homozygous germline *HOIP* mutation. (A) Amylopectin accumulation in bowel tissue from HOIP-deficient patient. Patient sternocleidomastoid muscular biopsy was stained with hematoxylin and eosin (H&E), or with periodic acid-Schiff stain (PAS) after diastase pretreatment (PASD). A patchy accumulation of PAS+diastase-resistant material in a scattered muscle fibers is shown in patient' biopsy. Bar, 50 µm. (B) Pedigree of the kindred, showing segregation of the L72P missense mutation. (C) *HOIP* DNA sequence electropherograms, for controls, the patient and her family. (D) Schematic diagram of the LUBAC complex. The domains identified are depicted as boxes: PNGase/UBA or UBX (PUB), ubiquitin-like (UBL), novel zinc-finger (NZF), really interesting new gene (RING) domain, in-between RING (IBR) domain, zinc finger (ZF). The red star indicates the position of the L72P mutation. Double arrows indicate the domain involved in the interaction between subunits. (E) Amino acid sequences alignment of the PUB domain of HOIP orthologues. The L72 residue is highlighted in red. The hashtags indicate the amino acids conserved in all proteins containing a PUB domain.

in HOIL-1 and SHARPIN. The HOIP missense mutation affects the conserved PUB domain of HOIP (Fig. 1 E), which has recently been shown to be important for the interaction of HOIP with OTULIN and CYLD, two deubiquitinases (Elliott et al., 2014; Fujita et al., 2014; Schaeffer et al., 2014). SIFT and Polyphen algorithms predicted a deleterious impact of this mutation on the function of the N-terminal domain (Table S2). Finally, the combined annotation dependent depletion score, a method for integrating many diverse annotations into a single measure (Kircher et al., 2014), predicted a deleterious impact of the L72P missense mutation (score of 22.2). Moreover, the *HOIP* gene does not harbor overtly deleterious mutations (nonsense, indels, essential splice mutations) at MAF higher than 1/100,000 in public and in-house databases, further suggesting that homozygosity for the L72P HOIP mutation could be disease-causing in the patient.

Impaired HOIP and LUBAC expression

We first assessed the impact of the mutation by analyzing *HOIP* mRNA levels by reverse transcription-quantitative PCR in SV40-transformed fibroblasts from patients and controls. The patient's cells contained ~50% less *HOIP* mRNA than control cells (Fig. 2 A). This mutation is located close to the acceptor splicing site of exon 2 (+6). We therefore also amplified and sequenced the full-length cDNA, but no splicing defect was detected (unpublished data). Examination of HOIP protein levels by immunoblotting revealed that no mutant protein was detected (Fig. 2 B) in patient's fibroblasts and EBV-B–transformed cells. We failed to restore the expression of the HOIP L72P protein in the patient's fibroblasts by inhibiting proteasome-, lysosome-, or autophagy-mediated protein clearance with MG-132, leupeptin, or 3-Methyladenine, respectively (unpublished data). This suggests that translation of HOIP L72P mRNAs, or stability of nascent L72P proteins, or both, is impaired. LUBAC contains three subunits: HOIP, HOIL-1, and the SHANK-associated RH domain-interacting protein (SHARPIN; Kirisako et al., 2006; Iwai and Tokunaga, 2009; Gerlach et al., 2011; Ikeda et al., 2011; Tokunaga et al., 2011; Stieglitz et al., 2013). We assessed the abundance of the other two components of LUBAC in control and patient's fibroblasts and EBV-B cells. SHARPIN and HOIL-1 protein levels were lower in the cells from the patient than in control cells (Fig. 2 B). We investigated the composition of LUBAC in the patient's cells further by performing immunoprecipitation experiments with antibodies against HOIP and SHARPIN, and monitoring the levels of the other two components of the complex. Only trace amounts of HOIP were detected in the patient's fibroblasts

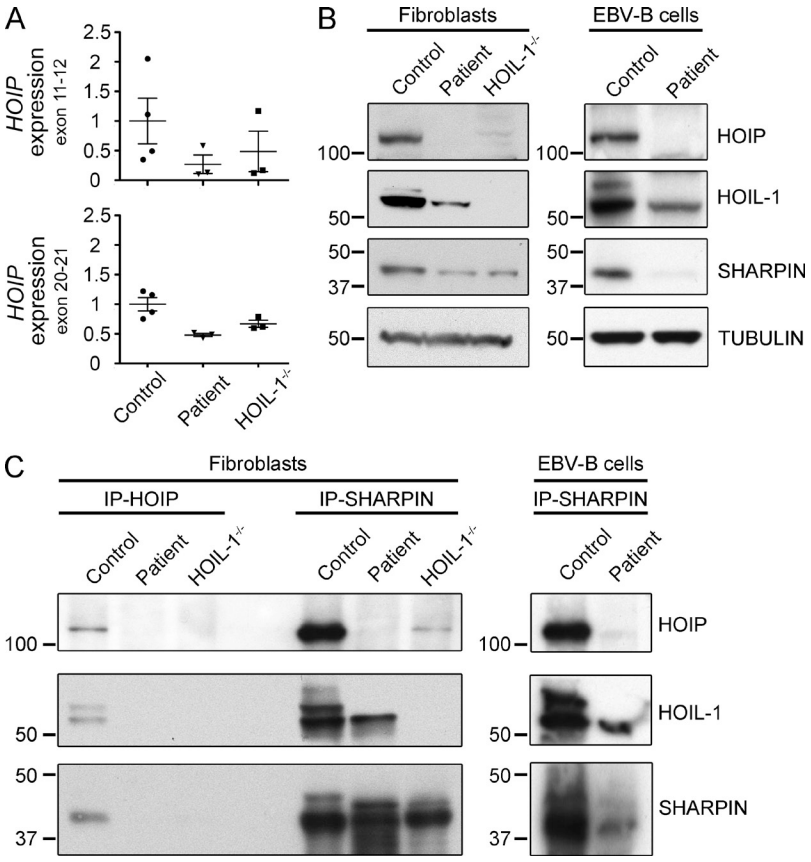

Figure 2. HOIP deficiency. (A) Relative HOIP mRNA levels in SV40-immortalized fibroblasts from controls, the HOIP-deficient patient (Patient), and HOIL-1–deficient patients (two independent experiments). (B) Expression of LUBAC subunits in control, HOIP-, and HOIL-1–deficient fibroblasts (left) and control and HOIP-deficient EBV-B cells (right) by immunoblotting total cell extracts with the indicated antibodies (two independent experiments). (C) Immunoblot of immunoprecipitated extracts from control, HOIP-, and HOIL-1–deficient fibroblasts (left) and control and HOIP-deficient EBV-B cells (right) with antibodies directed against HOIP (IP-HOIP) or SHARPIN (IP-SHARPIN) and detected with HOIL-1, HOIP, or SHARPIN antibodies (two independent experiments).

and EBV-B cells (Fig. 2 C). However, HOIL-1 and SHARPIN were still found to be associated as previously shown (Ikeda et al., 2011). Interestingly, although HOIL-1 was detected as a doublet in SDS-PAGE gels for control cells, only the lower MW product was associated with SHARPIN in the patient's cells (Fig. 2 B). Thus, the L72P mutation destabilizes the HOIP protein and, consequently, the overall LUBAC complex. These findings suggest that the L72P allele of HOIP is almost loss-of-expression.

Impaired NF-κB activation in the patient's fibroblasts

LUBAC regulates activation of the canonical NF-κB pathway, which plays a key role in inflammatory and immune responses (Tokunaga et al., 2009; Gerlach et al., 2011). We therefore assessed the functionality of the canonical NF-κB pathway in patient-derived SV40-transformed fibroblasts. Cells from a HOIL-1–deficient patient were also included in this study (Boisson et al., 2012). The HOIP-mutated patient's fibroblasts displayed impaired IKK phosphorylation and delayed IκBα degradation in response to TNF or IL-1β, as observed for HOIL-1–deficient fibroblasts (Fig. 3 A). These cells also displayed a marked impairment of IL-6 production after stimulation with TNF and IL-1β, as shown by ELISA (Fig. 3 B). Again, these findings were similar to those for HOIL-1–deficient cells. Using confocal microscopy, we recently showed that, in response to cytokine stimulation, the IKK complex is rapidly and transiently relocalized and activated into supramolecular complexes (Tarantino et al., 2014), which act as a marker of the early steps of NF-κB activation. As already reported for HOIL-1–deficient fibroblasts (Tarantino et al., 2014), we found that the IL-1 β–induced formation of NEMO-containing structures was almost entirely abolished in HOIP L72P-expressing fibroblasts (Fig. 3 C), whereas NEMO-containing complexes formed normally in the same cells treated with TNF. Finally, we examined the formation of linear polyubiquitin chains in control and HOIP-deficient fibroblasts treated with cytokines. Using an antibody that specifically recognizes linear polyubiquitin linkages (Matsumoto et al., 2012), we detected linear polyubiquitin aggregates in TNF- and IL-1β–treated control cells, but almost none in the patient's cells (Fig. 3 D). Overall, these data indicate that linear ubiquitination and NF-κB activation by IL-1β and TNF is impaired in fibroblasts from the patient with the *HOIP* mutation. Moreover, the IL-1β response is more severely affected than the TNF response, as previously shown for HOIL-1 deficiency (Boisson et al., 2012). Overall, these findings show that the fibroblastic phenotype of HOIP-mutated patients is as severe as that of HOIL-1–deficient patients, suggesting that the HOIP allele is at least strongly hypomorphic and perhaps completely loss-of-function.

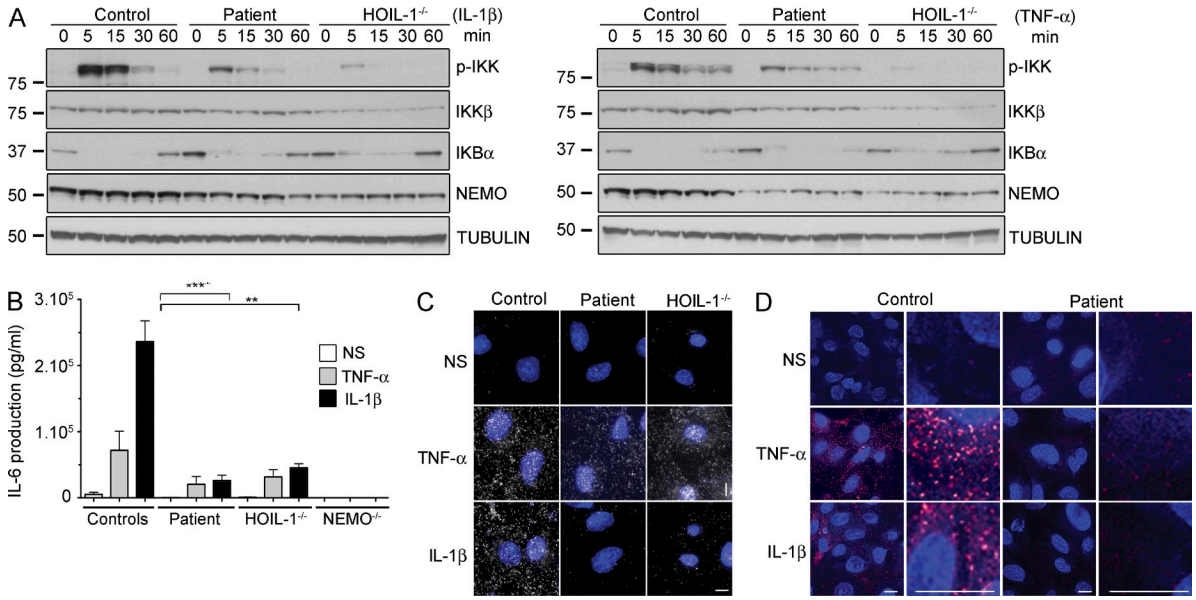

Figure 3. Impaired TNF- and IL-1β-induced NF-κB activation in the HOIP-deficient patient. (A) Time-course of IL-1β–stimulated (left) or TNF-stimulated (right) SV40-immortalized fibroblasts from control, HOIP-, and HOIL-1–deficient patients, with immunoblotting for phospho-IKK (p-IKK), IKKβ, IκBα, NEMO, and β-tubulin. (B) IL-6 production upon stimulation with TNF and IL-1β in SV-40 fibroblasts from two controls, HOIP- (Patient), HOIL-1–, and NEMO-deficient patients (errors bars indicate the SEM; 3 independent experiments). Unpaired Student's *t* tests were performed for the statistical analysis (**, $P < 0.01$; ***, $P < 0.001$). (C) Impaired recruitment of NEMO to punctate structures in the patient's fibroblasts. TNF- or IL-1β–stimulated cells were permeabilized with saponin before fixation, and immunolocalization with anti-NEMO antibody (white) was performed. Nuclei were stained with DAPI. Bar, 10 µm. (D) Absence of linear polyubiquitination in the patients' fibroblasts upon TNF or IL-1β stimulation. Immunolocalization with anti-linear ubiquitin chains antibody (red) was performed as in C. Nuclei were stained with DAPI. Bars, 10 µm.

Restoration of LUBAC stability and NF-κB activation by the wild-type *HOIP* allele

The L72P missense mutation is responsible for the destabilization of HOIP and, consequently, of the other two LUBAC subunits and the whole LUBAC complex, impairing NF-κB responses. In an attempt to rescue the biochemical and cellular phenotype, we reintroduced WT HOIP (N-terminally tagged), by retroviral transduction, into control, HOIP-, and HOIL-1–deficient fibroblasts. This genetic complementation led to the reappearance of the higher molecular weight HOIL-1 protein species on immunoblots (Fig. 4 A). It also led to the stabilization of SHARPIN not only in patient cells, but also in HOIL-$1^{-/-}$ cells. Moreover, it led to an increase in the phosphorylation of IKK kinases and faster IκBα degradation, similar to that reported for control cells stimulated with TNF or IL-1β (Fig. 4 B). Finally, cells from the patient complemented with the WT *HOIP* allele produced similar amounts of IL-6 to control cells in response to stimulation with TNF or IL-1β (Fig. 4 C). In contrast, the introduction of WT *HOIP* into HOIL-1–deficient cells did not restore the production of IL-6 in response to stimulation with TNF or IL-1β, highlighting the nonredundant role of HOIL-1 and HOIP in NF-κB activation (Fig. 4 C). Overall, these data confirm that the missense L72P mutation of *HOIP* is responsible for both the destabilization of LUBAC and the impairment of NF-κB activation in fibroblasts.

HOIP-deficient B cells do not respond to CD40L stimulation

The HOIP-deficient patient has hypogammaglobulinemia and nonprotective antibody responses to *Streptococcus pneumoniae* and *Haemophilus influenzae*. LUBAC has been shown to be important for the activation of B cells via the CD40 pathway in mice (Hostager et al., 2010, 2011; Sasaki et al., 2013) and in humans (Boisson et al., 2012). We therefore investigated the possible impairment of CD40 signaling in primary B cells from the HOIP-deficient patient. The stimulation of control B cells with CD40L plus IL-21 or CD40L plus IL-4 led to an increase in CD80 expression, as previously reported (Kennedy et al., 1994). In contrast, a marked impairment of CD80 up-regulation was observed with B cells from the patient (Fig. 5 A). Nevertheless, they were able to respond to BCR stimulation (anti-IgM plus CpG ± BAFF), suggesting that BCR activation is only partially dependent on LUBAC (Fig. 5 A). Stimulation of PBMCs with CD40L plus IL-21 is also known to induce differentiation of primary naive B cells to plasmablasts (Recher et al., 2011). We therefore explored plasmablast generation after stimulation of control and patient PBMCs with CD40L plus IL-21. After 7 d, the proportion of $CD19^{+}$ B cells that were also $CD27^{hi}$ $CD38^{hi}$ (identifying plasmablasts) was markedly lower for the patient than for the control (Fig. 5 B). We further tested the activation of the canonical NF-κB pathway upon stimulation by CD40L in EBV-B cells from the patient. We found reduced IκBα degradation and impaired phosphorylation of IKKs in HOIP-mutated

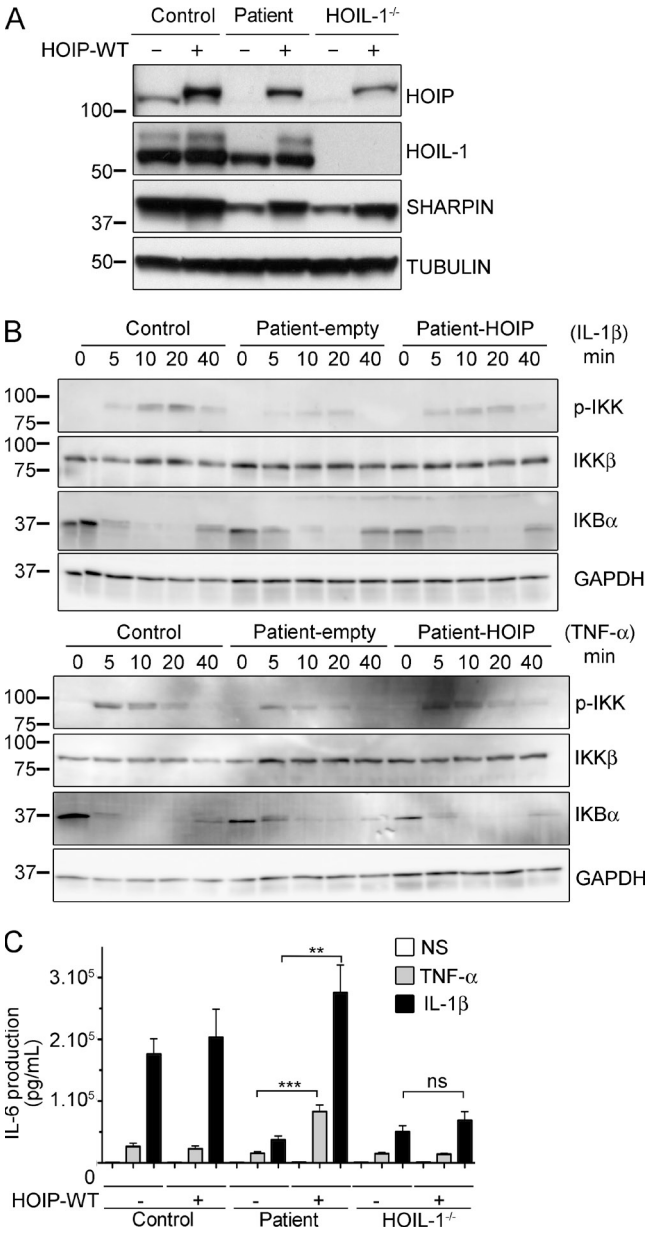

Figure 4. Complementation of impaired NF-κB activation by reintroduction of the WT *HOIP* allele. (A) Immunoblot of the three LUBAC subunits in SV-40–immortalized fibroblasts from control, HOIP-deficient (Patient), and HOIL-1–deficient cells expressing empty vector (-) or WT-V5 HOIP constructs (+). (B) Time course of IL-1β–stimulated (top) or TNF-stimulated (bottom) SV-40–immortalized fibroblasts from control, HOIP-deficient (Patient-empty), and HOIP-deficient cells complemented with WT HOIP (Patient-HOIP), with immunoblotting for p-IKK, IKKβ, IκBα, and GAPDH. (C) IL-6 production in SV-40 fibroblasts from control, HOIP-(Patient), or HOIL-1–deficient patients without (-) and with (+) WT HOIP complementation, after stimulation with TNF or IL-1β. Errors bars represent the SEM (five independent experiments). Unpaired Student's *t* tests were used for the statistical analysis (**, $P < 0.01$; ***, $P < 0.001$; ns, not significant).

cells, when compared with abolished signalization in CD40-deficient cells and normal signalization in control cells (Fig. 5 C). HOIP is thus essential for CD40 activation in human B cells, perhaps accounting at least in part for the patient's hypogammaglobulinemia and nonprotective antibody responses to *S. pneumoniae* and *H. influenzae*.

Enhanced response to IL-1β in HOIP-deficient monocytes

We then investigated the cellular basis for the inflammatory phenotype observed in the HOIP-deficient patient (see case report in Discussion). Upon stimulation in vitro with IL-1β for 48 h, the patient's PBMCs produced similar amounts of IL-6 and IL-10 than controls (Fig. 6 A). In contrast, the patient's cells failed to produce IL-10 in response to TNF (Fig. 6 A). Monocytes from HOIL-1–deficient patients have been reported to be hyperresponsive to IL-1β, probably accounting for the clinical autoinflammation observed in these patients (Boisson et al., 2012). We thus investigated the response of various leukocyte subsets from the HOIP-deficient patient, healthy controls, and IRAK4-deficient patients to in vitro stimulation with TNF, IL-1β, LPS, or a combination of PMA, ionomycin, and CpG-B. The various PBMC subsets were identified on the basis of cell surface expression of the following markers: CD3 (T cells), CD19 (B cells), CD56 (NK cells), and CD14 (monocytes). The production of IL-6, IL-8, MIP-1α, MIP-1β, IL-1β, and IFN-γ was assessed by intracellular staining and flow cytometry. Upon IL-1β stimulation, the proportion of monocytes producing IL-6 and IL-1β was higher in the patient than in healthy controls (13.1 ± 4% vs. 4.4 ± 1.0%, and 29.7 ± 8% vs. 13.8 ± 1.8%, respectively), whereas IRAK-4–deficient monocytes were unresponsive (Fig. 6 B). Moreover, the patient's monocytes produced IL-8 and MIP-1β in amounts similar to those for the control (Fig. 6 B). In conclusion, whole blood and PBMCs from the HOIP-deficient patient appear to respond strongly to IL-1β, like HOIL-1–deficient cells, potentially accounting for the clinical autoinflammation observed in this patient.

DISCUSSION

We have identified the first case of autosomal recessive HOIP deficiency in a patient with systemic autoinflammation, combined immunodeficiency, systemic lymphangiectasia, and mild amylopectinosis. Our study fulfills the criteria for genetic studies in single patients (Casanova et al., 2014). HOIP, HOIL-1, and SHARPIN are the three components of LUBAC, the E3-ligase complex responsible for linear ubiquitination (Iwai and Tokunaga, 2009; Gerlach et al., 2011; Ikeda et al., 2011; Tokunaga et al., 2011). We found that L72P mutation destabilized HOIP and, consequently, SHARPIN and HOIL-1. This situation is reminiscent of humans with inherited HOIL-1 deficiency (Boisson et al., 2012). In *Hoil1* (Tokunaga et al., 2009), *Sharpin* (Gerlach et al., 2011), and *Hoip* (Peltzer et al., 2014) knockout mice, and in B cell-specific conditional *Hoip* knockout mice (Sasaki et al., 2013), the absence of one subunit of LUBAC impairs the expression of the other two subunits, suggesting that LUBAC is a ternary complex in both mice and humans. LUBAC is involved in the NF-κB pathway, in which it conjugates linear polyubiquitin chains to specific Lys residues of NEMO (Tokunaga et al., 2009) and

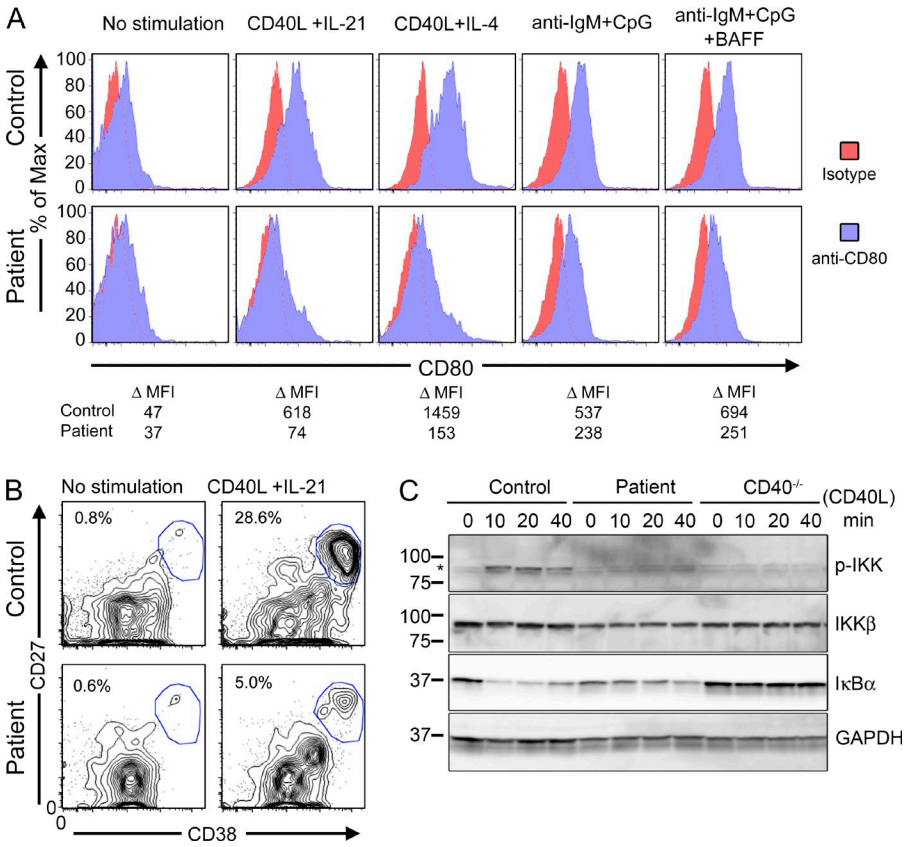

Figure 5. Impaired B cell activation in the HOIP-deficient patient. (A) Flow cytometry analysis of CD80 expression from stimulated PBMCs. PBMCs left unstimulated or stimulated for 3 d as indicated were stained for CD19 and with either an isotype control (red histograms) or an antibody directed against CD80 (blue histograms). CD80 expression values (CD80 median, isotype median) are indicated under the histograms (one experiment). (B) Flow cytometry analysis of CD27/CD38 expression on gated CD19+ cells, upon stimulation of PBMCs for 7 d with CD40L+IL-21 or with medium alone. The gated populations in the figure correspond to CD38hi and CD27hi plasmablasts (one experiment). (C) Time course of CD40L-stimulated EBV-immortalized B cells from control, HOIP- (patient), and CD40-deficient ($CD40^{-/-}$) patients, followed by immunoblotting for p-IKK, IKKβ, IκBα, and GAPDH (two independent experiments).

RIP1 (Gerlach et al., 2011). This activity is essential for full NF-κB activation in mice (Tokunaga et al., 2009; Ikeda et al., 2011; Zak et al., 2011). We showed in human HOIP-deficient fibroblasts that LUBAC expression and TNF- and IL-1β–driven NF-κB activation are impaired, as in HOIL-1–deficient patients. We also showed that linear ubiquitination is actually abolished in HOIP-deficient fibroblasts, which we had shown only recently for HOIL-1 deficiency (Boisson et al., 2012;

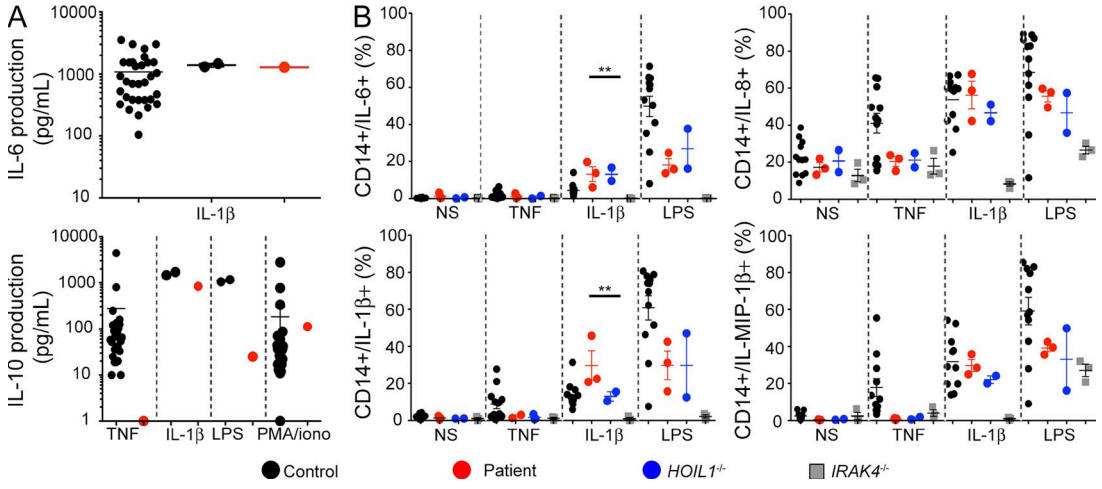

Figure 6. Hyperproduction of IL-6 upon IL-1β stimulation in HOIP-deficient monocytes. (A) Production of IL-6 and IL-10 by whole blood cells after 48 h of stimulation with TNF, IL-1β, LPS, and PMA/ionomycin in 32 controls (left), 2 travel controls (middle), and the HOIP-deficient patient (right, in red, 1 experiment). (B) Cytokine production in CD14+ cell subsets, as determined by intracellular FACS staining of stimulated PBMCs. PBMCs from 12 healthy controls (black), the HOIP-deficient patient (red), an HOIL-1–deficient patient (blue), and an IRAK-4–deficient patient (gray) were stimulated with TNF, IL-1β, or LPS. The secretory pathways were concomitantly blocked with monensin and Brefeldin A. 12 h after stimulation, the cells were immunolabeled with antibodies against CD14 and then permeabilized to assess the production of IL-6, IL-1β, IL-8, and MIP-1β by intracellular immunostaining. Labeled cells were analyzed by flow cytometry (3 independent experiments; **, $P < 0.01$).

Tarantino et al., 2014), connecting this biological activity with NF-κB activation in humans. Overall, our results demonstrate that human HOIP and HOIL-1 are both essential for LUBAC activity and for TNF-, IL-1β–, and CD40L-induced NF-κB responses, at least in fibroblasts and B cells.

This HOIP-deficient patient displayed autoinflammation, like three patients with HOIL-1 deficiency (Boisson et al., 2012). The apparent lack of autoinflammation (and immunodeficiency) in most of the other patients carrying bi-allelic mutations in HOIL-1 (Nilsson et al., 2013; Wang et al., 2013) may result from insufficient clinical characterization from at least one mutant allele being hypomorphic, from the impact of genetic modifiers, or from differences in the exposure to microbial infections (MacDuff et al., 2015). At any rate, the unusual association of IL-1β hyporesponsiveness in fibroblasts and hyperresponsiveness in monocytes from HOIP- or HOIL-1–deficient patients may be responsible for autoinflammation. In particular, we confirmed that the absence of LUBAC (or its presence in only very small amounts) leads to the overexpression of inflammatory genes and IL-1β hyperresponsiveness in mononuclear leukocytes, including monocytes in particular. *Hoip*$^{-/-}$ mice die during embryonic development (Sasaki et al., 2013; Peltzer et al., 2014), unlike *Hoil1*$^{-/-}$ and *Sharpin*$^{-/-}$ mice (HogenEsch et al., 1993; Tokunaga et al., 2009). The HOIP-deficient patient has several features in common with *Hoil1*$^{-/-}$ (MacDuff et al., 2015) and *Sharpin*$^{-/-}$ mice (HogenEsch et al., 1999, 2001; Seymour et al., 2007; Gerlach et al., 2011; Ikeda et al., 2011; Liang et al., 2011; Tokunaga et al., 2011), which display chronic severe eosinophilic inflammation. The production of proinflammatory cytokines upon IL-1β stimulation was not investigated in monocytes from *Sharpin* knockout mice, but the inflammatory phenotype of these mice was partially rescued by *Il1rap* (Liang et al., 2011) or *Tnf* (Gerlach et al., 2011) inactivation, or treatment with the proteasome inhibitor bortezomib, which inhibits NF-κB activation (Liang et al., 2011). The autoinflammation associated with LUBAC deficiency may be caused by NF-κB over-activation in response to certain stimuli in some cell types. These data provide interesting possibilities for therapeutic intervention.

Both HOIL-1– and HOIP-deficient patients had neonatal bacterial infections and impaired antibody response to *S. pneumoniae* and *H. influenzae* (Boisson et al., 2012). The HOIP-deficient patient also presented a broad impairment of antibody production not seen in HOIL-1–deficient patients, a slight excess of naive and transitional B cells and distinctive defects of CD40-dependent B cell activation and plasmablast differentiation. Interestingly, B cell-specific *Hoip* knockout mice have low levels of peritoneal B1 cells and markedly decreased serum levels of all immunoglobulin isotypes, probably due to a defect of the CD40 pathway (Sasaki et al., 2013). Moreover, the HOIP-deficient patient had severe T cell lymphopenia, affecting the naive compartment in particular, accompanied by an increase in the proportions of effector memory $CD4^+$ and T_{EMRA} $CD8^+$ cells. These abnormalities have not been observed in patients with HOIL-1 deficiency. However, in the Jurkat T cell line, HOIP knockdown impairs NF-κB activation upon TCR activation (Dubois et al., 2014). Moreover, human inborn defects of NF-κB signaling can lead to T cell defects, as seen with IκBα gain-of-function (Courtois et al., 2003) or IKKβ loss-of-function mutations (Pannicke et al., 2013; Mousallem et al., 2014; Nielsen et al., 2014). Overt T cell deficiency is more rarely seen in patients with hypomorphic mutations in NEMO (Döffinger et al., 2001; Casanova et al., 2011). Overall, inborn errors of LUBAC, like inborn errors of NF-κB, may underlie T cell deficiencies, a feature that apparently depends on the nature of the disease-causing gene.

Systemic lymphangiectasia may have also contributed to T cell lymphopenia in this patient, by lymphatic leak (Fuss et al., 1998). Lymphangiectasia has not been observed in HOIL-1–deficient patients (Boisson et al., 2012; Nilsson et al., 2013; Wang et al., 2013) and in *Hoil*$^{-/-}$ mice (Tokunaga et al., 2009). Although lymphangiectasia has not been reported in *Sharpin*$^{-/-}$ mice, they display dilation of the dermal, mouth, esophagus, and stomach capillaries (HogenEsch et al., 1993), similar to this patient's intestinal capillaries (see Case report). Moreover, *Hoip*$^{-/-}$ mice die in utero due to disrupted vasculature caused by TNFR1-mediated endothelial cell death (Peltzer et al., 2014). Conditional endothelial cell IKKβ KO mice also exhibit increased vasculature permeability (Ashida et al., 2011). Improper TNFR1 signaling seems to activate aberrant responses, in particular the formation of cytoplasmic complex II, triggering cell death. Overall, the circulatory and lymph vessel phenotypes of *Hoip*-deficient mice and HOIP-deficient patients suggest that HOIP, alone or less likely as a subunit of LUBAC, may regulate these systems. Finally, the HOIP-deficient patient displayed patches of cellular amylopectinosis, with muscular weakness at the lower extremities, but normal electromyography, and without clinical or echographic signs of cardiomyopathy. This contrasts with HOIL-1–deficient patients, whose amylopectinosis was an early onset, severe, and consistent manifestation, even in patients whose mutations were not proven to be loss-of-function (Boisson et al., 2012; Nilsson et al., 2013; Wang et al., 2013). The milder amylopectinosis in the HOIP-deficient patient suggests that amylopectinosis may be more dependent on HOIL-1 than HOIP, LUBAC, and NF-κB. Alternatively, the HOIP L72P mutation may not be completely loss-of-function.

Case report

The patient, a 19-yr-old woman of Kuwaiti origin, was born at term, after a twin pregnancy. Her parents are first cousins and her twin brother is healthy. During the neonatal period, she presented omphalitis, requiring antibiotic treatment, and splenomegaly. After discharge, she had recurrent episodes of fever and persistent splenomegaly, associated with mild liver enlargement. At the age of 2 yr, familial Mediterranean fever was suspected, leading to the treatment of the patient for 3 yr with colchicine, with no clinical benefit. From early childhood, the growth of the patient was stunted. At the age of 4 yr, she developed generalized lymphadenopathy after

immunization with BCG. 1 yr later, she presented severe respiratory distress, requiring mechanical ventilation. Treatment with rifampicin was initiated for possible mycobacterial disease. At the age of 7 yr, the patient began to suffer from recurrent episodes of fatty diarrhea, associated with fever and oral ulcers. Immunological investigations were performed for the first time at the age of 9 yr and showed T cell lymphopenia ($CD3^+$: 776 cells/µl), an impaired proliferative response to anti-CD3 (cpm: 1,106 vs. 35,216 in a normal control), and hypogammaglobulinemia (IgG: 315 mg/dl), associated with nonprotective antibody responses to *S. pneumoniae* and *H. influenzae*, but with a good antibody response to tetanus toxoid. Prophylaxis with cotrimoxazole was initiated. Additional abnormalities identified in laboratory tests included hypoalbuminemia (2.6 g/dl), hypocalcemia (8.2 mg/dl), anemia (Hb, 8.1 g/dl), iron deficiency (3.7 µmol/l), vitamin 25-OH D3 deficiency (7 nmol/l; n.v., 75–125 nmol/l), and an elevated ESR (97 mm/h) and high C-reactive protein (CRP) serum level (8.06 mg/dl). Endoscopies of the upper and lower gastrointestinal tract were unremarkable. The poor growth of the patient led to treatment with human recombinant growth hormone (hrGR). However, this treatment was complicated by femur fractures, leading to its cessation. At 15 yr of age, the patient complained of severe pain in the hips, knees, and ankles. Treatment with a nonsteroidal antiinflammatory drug (naproxen) led to clinical improvement, but was complicated by gastrointestinal bleeding. Recurrent episodes of diarrhea and edema, requiring frequent infusions of albumin and furosemide, led to additional investigations. Negative results were repeatedly obtained for endoscopy, but videocapsule endoscopy, at the age of 16 yr, showed patchy areas of white-tipped thickened villi throughout most of the small bowel, consistent with intestinal lymphangiectasia. Further evidence of lymph vessel abnormalities was provided by a lymphangiogram (showing abnormal filling of the thoracic duct), high α-1-antitrypsin antibody, and triglyceride concentrations. The patient was placed on a low-fat, high-protein diet, with some improvement, but she continued to suffer from fatty diarrhea, with poor weight gain and impaired linear growth. She also developed persistent warts. A chest CT scan at the age of 17 yr demonstrated mild bronchiectasis in the right middle and lower lobes. Laboratory examinations at 18 yr of age confirmed the T and B cell abnormalities (Table S2), associated with elevated fluctuating but consistently high ESR (between 26 and 119 mm/h), increased CRP concentration (between 1.22 and 12.68 mg/dl; normal values: ≤0.5 mg/dl), and haptoglobin concentration (275 mg/dl; normal range: 33–183 mg/dl). Treatment with intravenous immunoglobulins was initiated, leading to an improvement in IgG trough levels. However, the episodes of systemic edema persisted, although at a lower frequency. The most recent follow-up visit showed a worsening of intestinal lymphangiectasia. An endoscopy with biopsies showed dilated lymphatic space in duodenal, small intestinal, and colonic mucosa. Moreover, the patient was suffering from muscular weakness, especially in the lower extremities. An MRI of the pelvis demonstrated diffuse muscular atrophy, with fatty infiltration of the gluteal musculature and the abductors. However, motor and sensory conduction and needle electromyography were normal, and there was no evidence of cardiomyopathy at heart ultrasound. Creatine phosphokinase (CK) and LDH levels are within the normal limits. Pulmonary function tests have shown reduced forced expiratory volume (78% of predicted), but to a lower extent than has been reported in HOIL-1 deficient patients. The patient is still on antibiotic prophylaxis, a low-fat and high-protein diet, iron and vitamin D supplementation, and immunoglobulin replacement therapy, and has started treatment with octreotide.

MATERIALS AND METHODS

Sample collection. This study was conducted in accordance with the Helsinki Declaration, with informed consent obtained from the patient and her family. The study was approved by the local ethics committee of Necker-Enfants Malades Hospital (Paris, France); Boston Children Hospital (Boston, MA); and The Rockefeller University Hospital (New York, NY).

Genetic analysis. For WES massively parallel sequencing, genomic DNA extracted from the patient's peripheral blood cells was sheared with a Covaris S2 Ultrasonicator. An adapter-ligated library was prepared with the Paired-End Sample Prep kit V1 (Illumina). Exome capture was performed with the SureSelect Human All Exon kit (Agilent Technologies). Paired-end sequencing was performed on a HiSeq 2500, generating 100-base reads. For sequence alignment, variant calling and annotation, we used BWA aligner (Li and Durbin, 2009) to align sequences with the human genome reference sequence (hg19 build). Downstream processing was performed with the Genome analysis toolkit (GATK; McKenna et al., 2010), SAMtools (Li et al., 2009), and Picard Tools. Substitution and indel calls were identified with a GATK Unified Genotyper and a GATK Indel GenotyperV2, respectively. All calls with a read coverage ≤2x and a Phred-scaled SNP quality of ≤20 were filtered out. All the variants were annotated with the GATK Genomic Annotator.

For genotyping and linkage analysis, the patient, her parents, and her unaffected brother were genotyped with the Affymetrix GeneChip Human Mapping 250K array. Genotype calling was achieved with Power Tools (Affymetrix). We discarded monomorphic single-nucleotide polymorphisms (SNPs), SNPs with a call rate <100%, and SNPs presenting more than one Mendelian inconsistency within the family. SNPs were further filtered based on population-based filters, using HapMap CEU trios. Multipoint linkage analysis, assuming autosomal recessive inheritance with complete penetrance (homozygosity mapping), was performed using Merlin software (Abecasis et al., 2002) on 84,954 high-quality SNPs. Marker–marker linkage disequilibrium was modeled by creating clusters including SNPs for which pairwise r^2 was greater than 0.4 and all intervening SNPs (Abecasis and Wigginton, 2005). The HapMap CEU trios were used to estimate pairwise r^2 and haplotype frequencies of the clusters. We used different genomic database: Exome Aggregation Consortium (ExAC), 1000 Genome Project, and dbSNP all accessed in February 2015. CADD score for variation was calculated using the University of Washington's CADD website.

Cell lines, immortalization, and complementation. Control and patient-derived fibroblasts were immortalized by transfection with a plasmid encoding the SV40 large-T antigen. Transformed cell lines were grown in DMEM (Invitrogen) supplemented with 10% fetal calf serum (Invitrogen). The human $NEMO^{-/-}$ fibroblasts were provided by A. Smahi (Imagine Institute, Paris, France; Smahi et al., 2000). The HOIP-V5 open-reading frame was amplified from a plasmid provided by Henning Walczak and inserted into the retroviral vector pMSCV (Life Science). Infectious viral particles were produced by cotransfecting GP2-293 packaging cells with pVSV-G and pMSCV-HOIP or an empty vector (Life Science). Viral particles were

collected 48–72 h after transfection and used to infect SV40-transformed fibroblasts. Infected cells were selected with 0.4 µg/ml puromycin (Invitrogen). B lymphocyte cell lines from the patient and a healthy donor have been immortalized with Epstein-Barr virus and grown in RPMI 1640 (Gibco) supplemented with 15% fetal calf serum (Invitrogen).

Antibodies and reagents. The antibodies used for detection on immunoblots were anti-HOIL-1 N-ter, provided by H. Walczak (University College London, London, England, UK; Haas et al., 2009), anti-HOIL-1 C-ter provided by K. Iwai (Graduate School of Medicine, Kyoto University, Kyoto, Japan; Kirisako et al., 2006), anti-HOIP (PAB6229; Abnova), and anti-linear polyubiquitin chains 1F113F5/Y102L provided by Genentech (Matsumoto et al., 2012), anti-NEMO (sc-8330; Santa Cruz Biotechnology, Inc.; #611306; BD), anti-SHARPIN (14626–1-AP; ProteinTech), anti-IκBα (#610690; BD), anti-phospho-IKKα-β (ser176/180; 16A6; Cell Signaling Technology), anti-IKKβ (AM8109a, Abgent), anti-β-tubulin (T4026; Sigma-Aldrich), and anti-GAPDH (sc-365062; Santa Cruz Biotechnology, Inc.) antibodies. Species-specific secondary antibodies coupled to horseradish peroxidase were obtained from Vector Laboratories or Amersham-Pharmacia.

Immunostaining. Periodic acid-Shift (PAS) staining was done using a standard clinical histopathology laboratory procedure. Sections of frozen tissue or formalin fixed from a sternocleidomastoid muscle biopsy were deparaffinized and rehydrated, then either rinsed in water or incubated with 1% diastase (Sigma-Aldrich) in distilled water for 60 min at 60°C, followed by rinsing in water for 2 min. Slides were then incubated with 0.5% periodic acid (Poly-Scientific R&D) for 5 min, rinsed four times in distilled water, placed in Schiff's solution (Poly-Scientific R&D) for 15 min, rinsed in tap water for 10 min, counterstained with Harris hematoxylin (Poly-Scientific R&D) for 5 min, and rinsed in water again for 5 min. After quick dipping in 0.5% acid alcohol, slides were extensively rinsed in water before dehydration, clearing, and mounting in permanent mounting media. The presence of amylopectinosis was documented by persistence of PAS-positive material in diastase-treated sections. Images have been captured with an BX43 microscope and DP25 digital camera (both from Olympus).

Cell lysis, immunoprecipitation, and immunoblotting. Cells were lysed in a buffer containing 30 mM Tris-HCl, pH 7.5, 120 mM NaCl, 2 mM KCl, 1% Triton X-100, and 2 mM EDTA supplemented with protease and phosphatase inhibitors (Complete and PhoStop; Roche). For immunoprecipitation, antibodies (5 µg) were added to 1 mg of total protein extract and incubated overnight at 4°C. Protein A– or protein G–coupled agarose beads (Sigma-Aldrich) were added to the samples, which were then incubated for 1 h at 4°C. Beads were washed three times in lysis buffer and resuspended in Laemmli buffer.

Immunofluorescence. For immunofluorescence, cells cultured on glass coverslips were treated twice with ice-cold saponin extraction buffer (80 mM Pipes, pH 6.8, 1 mM $MgCl_2$, 1 mM EGTA, and 0.1% saponin) for 2 min and 4 min on ice as previously described (Tarantino et al., 2014). Cells were then washed twice with PBS before fixation in 100% methanol. The cells were progressively rehydrated by successive washes with 85, 70, and 50% ethanol in water and two final washes with PBS. After blocking by incubation with 1% BSA in PBS, the slides were incubated with rabbit anti-NEMO antibodies or with human anti-linear polyubiquitin, washed with PBS and incubated either with anti–rabbit Alexa Fluor 488 or anti–human Alexa Fluor 546 secondary antibodies (Life Technologies). The slides were then washed again and incubated with DAPI (Sigma-Aldrich) to stain the nuclei. The coverslips were mounted in Mowiol supplemented with an anti-fading agent (AF100; Biovalley). Specimens were examined with an ApoTome imaging system (Imager Z1; Carl Zeiss) equipped with a 63×/1.4 oil DIC objective (Carl Zeiss).

Gene expression and qPCR analysis. RNA was extracted from SV40-transformed fibroblasts with TRIzol (Invitrogen) and reverse-transcribed (2 µg) with the SuperScript III first-strand synthesis kit (Invitrogen). HOIP expression was quantified by RT-qPCR in a *Taq*Man Gene Expression Assay (Hs00215938_m1, Hs01047328_g1; Life Technologies), with normalization against GUS probes.

Cell stimulation, ELISA, and FACS analysis. For whole blood activation, fresh blood was first mixed with an equal volume of RPMI-1640 (Invitrogen), left untreated, or treated with agonists for 48 h. Levels of IL-6 and IL-10 secretion were determined with ELISA kits (M9316 and M1910; Sanquin).

For B cell activation, PBMCs were purified by Ficoll gradient centrifugation, and 10^6 cells were cultured in 24-well plates within 1 ml RPMI medium per well supplemented with 10% FBS and 50 U/ml penicillin (Invitrogen) and 50 µg/ml streptomycin (Invitrogen). The cells were stimulated for 3 d with CD40L+IL-21, CD40L+IL-4, anti-IgM+CpG, or anti-IgM+Cpg+BAFF (5 µg/ml CD40L, 200 ng/ml IL-21-Fc, BAFF, anti-IgM [1 µg/ml; Southern Biotech], CpG [500 nM; Invivogen], and IL-4 [1 ng/ml; R&D Systems]). PBMCs were harvested, blocked by incubation for 10 min in PBS+10% human serum, and stained by incubation for 30 min on ice, for CD19 (BioLegend), an isotype control or CD80 (eBioscience). Flow cytometry analyses were performed on a BD LSRFortessa flow cytometer (BD). Cells were gated on $CD19^+$ and CD80 expression was then analyzed with FlowJo software (Tree Star).

For plasmablast assay, PBMCs were cultured in RPMI supplemented with 10% FBS, 0.025% Hepes, 0.01% PenStrep, 0.01% sodium pyruvate, 0.005% NEAA, 0.005% L-glutamine, and 0.0013% β-mercaptoethanol) alone (unstimulated cells) or with 200 ng/ml IL-21-Fc and 5 µg/ml CD40 ligand for a total of 7 d. Cells were stained with CD19-PECy5 (BioLegend; clone HIB19), CD27-APC (eBioscience; clone O323), or CD38-PECy7 (BioLegend; clone HIT2) antibodies, and analyzed by flow cytometry on an LSR II machine (BD) with FlowJo software (Tree Star).

For leukocyte activation, frozen PBMCs were washed twice with FCS-containing medium and used to seed 48-well plates (10^6 cells/well). They were cultured for 4–6 h, and then stimulated with TNF (20 ng/ml; R&D Systems) IL-1β (10 ng/ml; R&D Systems), LPS (10 ng/ml; Sigma-Aldrich), or PMA+ionomycin+CpGB (Sigma-Aldrich; 10^{-9} M + 10^{-7} M + 100 µg/ml). During stimulation, protein transport was blocked with GolgiStop and GolgiPlug (BD). Cells were stained with anti-CD3 (BD; #560366), anti-CD19 (BD; #340951), anti-CD14 (BD; #557742), and anti-CD56 (BioLegend; #318331) antibodies for cellular phenotyping and with Aqua Live/Dead (Invitrogen) to exclude dead cells. After fixation and permeabilization (BD; #554722), the cells were stained with antibodies against IL-6 (BD; #561441), MIP-1β (BD; #554730), MIP-1β (BD; #560565), IL-1β (BD; #340515), IL-8 (BD; #511410), and IFN-γ (BD; #559326). Stained PBMCs were captured by flow cytometry with a LSRII flow cytometer (BD) and FACSDiva software (BD). The data were analyzed with FlowJo software (Tree Star).

Statistics. GraphPad Prism software was used to conduct unpaired, two-tailed Student's *t* tests for sample analysis or one-way ANOVA followed by Tukey's multiple comparison test.Values of $P < 0.05$ were considered significant.

Online supplemental material. Table S1, available as an Excel file, shows the immunological profile of the patient. Table S2, available as an Excel file, shows whole-exome sequencing data for the patient. Online supplemental material is available at http://www.jem.org/cgi/content/full/jem.20141130/DC1.

We thank the child and her family for participating, and Drs. C. Hug, A. Taghinia, and L. Zimmerman for taking care of them. We particularly thank Drs H. Walczak, K. Iwai, and A. Smahi for kindly providing antibodies, recombinant proteins, and cells. We also thank Lacey Cardillo, Benjamin Ferland, Tatiana Kochetkov, and Adeline Crinier for technical assistance, and Jill de Jong and Mary Ellen Conley for scientific discussion. We finally thank Yelena Nemirovskaya, Eric Anderson, and Martine Courat for administrative assistance.

This work was partly funded by NCRR and NCATS, National Institutes of Health (8UL1TR000043), St. Giles Foundation, The Rockefeller University, Institut National de la Santé et de la Recherche Médicale, Paris Descartes University, NIH

(5P01AI061093; J.-L. Casanova), Canceropole Ile de France (2007; A. Israel), the "Fondation ARC pour la Recherche sur le Cancer" (SFI20121205641) and the "Ligue Contre le Cancer" (E. Laplantine), NIH (5P01AI076210; L.D. Notarangelo), NIH (5R01AI100887), the Manton Foundation (L.D. Notarangelo), the Dubai Harvard Foundation for Medical Research (W. Al-Herz and L.D. Notarangelo), and the Kuwait Foundation for the Advancement of Sciences (grant 2010-1302-05; W. Al-Herz).

The authors declare no competing financial interests.

Author contributions: B. Boisson, E. Laplantine, K. Dobbs, N. Tarantino, E. Tsitsikov, M. Chrabieh, C. Picard, L. Du, and G. Hopkins performed the experiments;. M. Hazen, W. Al-Herz, and L.D. Notarangelo took care of the patient. A. Cobat, A. Belkadi, Y. Itan, and L. Abel performed and analyzed the SNP arrays. H.G.W. Lidov and J.-C. Fournet supervised and analyzed the histology. B. Boisson, E. Laplantine, and S.-Y. Pai supervised experiments. L.D. Notarangelo identified and took care of the patient, and also planned and supervised experiments. E. Laplantine, J.-L. Casanova, A. Israel, and L.D. Notarangelo contributed to the writing of the manuscript. B. Boisson coordinated the study and wrote the manuscript. All authors discussed the results and commented on the manuscript.

Submitted: 14 June 2014
Accepted: 27 April 2015

REFERENCES

Abecasis, G.R., and J.E. Wigginton. 2005. Handling marker-marker linkage disequilibrium: pedigree analysis with clustered markers. *Am. J. Hum. Genet.* 77:754–767. http://dx.doi.org/10.1086/497345

Abecasis, G.R., S.S. Cherny, W.O. Cookson, and L.R. Cardon. 2002. Merlin—rapid analysis of dense genetic maps using sparse gene flow trees. *Nat. Genet.* 30:97–101. http://dx.doi.org/10.1038/ng786

Al-Herz, W., A. Bousfiha, J.L. Casanova, T. Chatila, M.E. Conley, C. Cunningham-Rundles, A. Etzioni, J.L. Franco, H.B. Gaspar, S.M. Holland, et al. 2014. Primary immunodeficiency diseases: an update on the classification from the international union of immunological societies expert committee for primary immunodeficiency. *Front. Immunol.* 5:162. http://dx.doi.org/10.3389/fimmu.2014.00162

Alitalo, K. 2011. The lymphatic vasculature in disease. *Nat. Med.* 17:1371–1380. http://dx.doi.org/10.1038/nm.2545

Allen, R.C., R.J. Armitage, M.E. Conley, H. Rosenblatt, N.A. Jenkins, N.G. Copeland, M.A. Bedell, S. Edelhoff, C.M. Disteche, D.K. Simoneaux, et al. 1993. CD40 ligand gene defects responsible for X-linked hyper-IgM syndrome. *Science.* 259:990–993. http://dx.doi.org/10.1126/science.7679801

Alsina, L., E. Israelsson, M.C. Altman, K.K. Dang, P. Ghandil, L. Israel, H. von Bernuth, N. Baldwin, H. Qin, Z. Jin, et al. 2014. A narrow repertoire of transcriptional modules responsive to pyogenic bacteria is impaired in patients carrying loss-of-function mutations in MYD88 or IRAK4. *Nat. Immunol.* 15:1134–1142. http://dx.doi.org/10.1038/ni.3028

Ashida, N., S. Senbanerjee, S. Kodama, S.Y. Foo, M. Coggins, J.A. Spencer, P. Zamiri, D. Shen, L. Li, T. Sciuto, et al. 2011. IKKβ regulates essential functions of the vascular endothelium through kinase-dependent and -independent pathways. *Nat. Commun.* 2:318. http://dx.doi.org/10.1038/ncomms1317

Boisson, B., and J.L. Casanova. 2014. LUBAC: A new function in immunity. *J. Exp. Med.* 211:1272. http://dx.doi.org/10.1084/jem.2117insight3

Boisson, B., E. Laplantine, C. Prando, S. Giliani, E. Israelsson, Z. Xu, A. Abhyankar, L. Israël, G. Trevejo-Nunez, D. Bogunovic, et al. 2012. Immunodeficiency, autoinflammation and amylopectinosis in humans with inherited HOIL-1 and LUBAC deficiency. *Nat. Immunol.* 13:1178–1186. http://dx.doi.org/10.1038/ni.2457

Boisson, B., P. Quartier, and J.L. Casanova. 2015. Immunological loss-of-function due to genetic gain-of-function in humans: autosomal dominance of the third kind. *Curr. Opin. Immunol.* 32:90–105. http://dx.doi.org/10.1016/j.coi.2015.01.005

Bolze, A., M. Byun, D. McDonald, N.V. Morgan, A. Abhyankar, L. Premkumar, A. Puel, C.M. Bacon, F. Rieux-Laucat, K. Pang, et al. 2010. Whole-exome-sequencing-based discovery of human FADD deficiency. *Am. J. Hum. Genet.* 87:873–881. http://dx.doi.org/10.1016/j.ajhg.2010.10.028

Byun, M., A. Abhyankar, V. Lelarge, S. Plancoulaine, A. Palanduz, L. Telhan, B. Boisson, C. Picard, S. Dewell, C. Zhao, et al. 2010. Whole-exome sequencing-based discovery of STIM1 deficiency in a child with fatal classic Kaposi sarcoma. *J. Exp. Med.* 207:2307–2312. http://dx.doi.org/10.1084/jem.20101597

Casanova, J.L., L. Abel, and L. Quintana-Murci. 2011. Human TLRs and IL-1Rs in host defense: natural insights from evolutionary, epidemiological, and clinical genetics. *Annu. Rev. Immunol.* 29:447–491. http://dx.doi.org/10.1146/annurev-immunol-030409-101335

Casanova, J.L., M.E. Conley, S.J. Seligman, L. Abel, and L.D. Notarangelo. 2014. Guidelines for genetic studies in single patients: lessons from primary immunodeficiencies. *J. Exp. Med.* 211:2137–2149. http://dx.doi.org/10.1084/jem.20140520

Conley, M.E., and J.L. Casanova. 2014. Discovery of single-gene inborn errors of immunity by next generation sequencing. *Curr. Opin. Immunol.* 30:17–23. http://dx.doi.org/10.1016/j.coi.2014.05.004

Courtois, G., A. Smahi, J. Reichenbach, R. Döffinger, C. Cancrini, M. Bonnet, A. Puel, C. Chable-Bessia, S. Yamaoka, J. Feinberg, et al. 2003. A hypermorphic IkappaBalpha mutation is associated with autosomal dominant anhidrotic ectodermal dysplasia and T cell immunodeficiency. *J. Clin. Invest.* 112:1108–1115. http://dx.doi.org/10.1172/JCI18714

DiSanto, J.P., J.Y. Bonnefoy, J.F. Gauchat, A. Fischer, and G. de Saint Basile. 1993. CD40 ligand mutations in x-linked immunodeficiency with hyper-IgM. *Nature.* 361:541–543. http://dx.doi.org/10.1038/361541a0

Döffinger, R., A. Smahi, C. Bessia, F. Geissmann, J. Feinberg, A. Durandy, C. Bodemer, S. Kenwrick, S. Dupuis-Girod, S. Blanche, et al. 2001. X-linked anhidrotic ectodermal dysplasia with immunodeficiency is caused by impaired NF-kappaB signaling. *Nat. Genet.* 27:277–285. http://dx.doi.org/10.1038/85837

Dubois, S.M., C. Alexia, Y. Wu, H.M. Leclair, C. Leveau, E. Schol, T. Fest, K. Tarte, Z.J. Chen, J. Gavard, and N. Bidère. 2014. A catalytic-independent role for the LUBAC in NF-κB activation upon antigen receptor engagement and in lymphoma cells. *Blood.* 123:2199–2203. http://dx.doi.org/10.1182/blood-2013-05-504019

Elliott, P.R., S.V. Nielsen, P. Marco-Casanova, B.K. Fiil, K. Keusekotten, N. Mailand, S.M. Freund, M. Gyrd-Hansen, and D. Komander. 2014. Molecular basis and regulation of OTULIN-LUBAC interaction. *Mol. Cell.* 54:335–348. http://dx.doi.org/10.1016/j.molcel.2014.03.018

Ferrari, S., S. Giliani, A. Insalaco, A. Al-Ghonaium, A.R. Soresina, M. Loubser, M.A. Avanzini, M. Marconi, R. Badolato, A.G. Ugazio, et al. 2001. Mutations of CD40 gene cause an autosomal recessive form of immunodeficiency with hyper IgM. *Proc. Natl. Acad. Sci. USA.* 98:12614–12619. http://dx.doi.org/10.1073/pnas.221456898

Fujita, H., S. Rahighi, M. Akita, R. Kato, Y. Sasaki, S. Wakatsuki, and K. Iwai. 2014. Mechanism underlying IκB kinase activation mediated by the linear ubiquitin chain assembly complex. *Mol. Cell. Biol.* 34:1322–1335. http://dx.doi.org/10.1128/MCB.01538-13

Fuss, I.J., W. Strober, B.A. Cuccherini, G.R. Pearlstein, X. Bossuyt, M. Brown, T.A. Fleisher, and K. Horgan. 1998. Intestinal lymphangiectasia, a disease characterized by selective loss of naive CD45RA+ lymphocytes into the gastrointestinal tract. *Eur. J. Immunol.* 28:4275–4285. http://dx.doi.org/10.1002/(SICI)1521-4141(199812)28:12<4275::AID-IMMU4275>3.0.CO;2-P

Gerlach, B., S.M. Cordier, A.C. Schmukle, C.H. Emmerich, E. Rieser, T.L. Haas, A.I. Webb, J.A. Rickard, H. Anderton, W.W. Wong, et al. 2011. Linear ubiquitination prevents inflammation and regulates immune signalling. *Nature.* 471:591–596. http://dx.doi.org/10.1038/nature09816

Haas, T.L., C.H. Emmerich, B. Gerlach, A.C. Schmukle, S.M. Cordier, E. Rieser, R. Feltham, J. Vince, U. Warnken, T. Wenger, et al. 2009. Recruitment of the linear ubiquitin chain assembly complex stabilizes the TNF-R1 signaling complex and is required for TNF-mediated gene induction. *Mol. Cell.* 36:831–844. http://dx.doi.org/10.1016/j.molcel.2009.10.013

HogenEsch, H., M.J. Gijbels, E. Offerman, J. van Hooft, D.W. van Bekkum, and C. Zurcher. 1993. A spontaneous mutation characterized by chronic proliferative dermatitis in C57BL mice. *Am. J. Pathol.* 143:972–982.

HogenEsch, H., S. Janke, D. Boggess, and J.P. Sundberg. 1999. Absence of Peyer's patches and abnormal lymphoid architecture in chronic proliferative dermatitis (cpdm/cpdm) mice. *J. Immunol.* 162:3890–3896.

HogenEsch, H., S.E. Torregrosa, D. Boggess, B.A. Sundberg, J. Carroll, and J.P. Sundberg. 2001. Increased expression of type 2 cytokines in chronic proliferative dermatitis (cpdm) mutant mice and resolution of inflammation following treatment with IL-12. *Eur. J. Immunol.* 31:734–742. http://dx.doi.org/10.1002/1521-4141(200103)31:3<734::AID-IMMU734>3.0.CO;2-9

Hostager, B.S., D.K. Fox, D. Whitten, C.G. Wilkerson, B.A. Eipper, V.P. Francone, P.B. Rothman, and J.D. Colgan. 2010. HOIL-1L interacting protein (HOIP) as an NF-kappaB regulating component of the CD40 signaling complex. *PLoS ONE*. 5:e11380. http://dx.doi.org/10.1371/journal.pone.0011380

Hostager, B.S., M. Kashiwada, J.D. Colgan, and P.B. Rothman. 2011. HOIL-1L interacting protein (HOIP) is essential for CD40 signaling. *PLoS ONE*. 6:e23061. http://dx.doi.org/10.1371/journal.pone.0023061

Ikeda, F., Y.L. Deribe, S.S. Skånland, B. Stieglitz, C. Grabbe, M. Franz-Wachtel, S.J. van Wijk, P. Goswami, V. Nagy, J. Terzic, et al. 2011. SHARPIN forms a linear ubiquitin ligase complex regulating NF-κB activity and apoptosis. *Nature*. 471:637–641. http://dx.doi.org/10.1038/nature09814

Itan, Y., S.Y. Zhang, G. Vogt, A. Abhyankar, M. Herman, P. Nitschke, D. Fried, L. Quintana-Murci, L. Abel, and J.L. Casanova. 2013. The human gene connectome as a map of short cuts for morbid allele discovery. *Proc. Natl. Acad. Sci. USA*. 110:5558–5563. http://dx.doi.org/10.1073/pnas.1218167110

Iwai, K., and F. Tokunaga. 2009. Linear polyubiquitination: a new regulator of NF-kappaB activation. *EMBO Rep.* 10:706–713. http://dx.doi.org/10.1038/embor.2009.144

Kennedy, M.K., K.M. Mohler, K.D. Shanebeck, P.R. Baum, K.S. Picha, C.A. Otten-Evans, C.A. Janeway Jr., and K.H. Grabstein. 1994. Induction of B cell costimulatory function by recombinant murine CD40 ligand. *Eur. J. Immunol.* 24:116–123. http://dx.doi.org/10.1002/eji.1830240118

Kircher, M., D.M. Witten, P. Jain, B.J. O'Roak, G.M. Cooper, and J. Shendure. 2014. A general framework for estimating the relative pathogenicity of human genetic variants. *Nat. Genet.* 46:310–315. http://dx.doi.org/10.1038/ng.2892

Kirisako, T., K. Kamei, S. Murata, M. Kato, H. Fukumoto, M. Kanie, S. Sano, F. Tokunaga, K. Tanaka, and K. Iwai. 2006. A ubiquitin ligase complex assembles linear polyubiquitin chains. *EMBO J.* 25:4877–4887. http://dx.doi.org/10.1038/sj.emboj.7601360

Lee, C.E., D.A. Fulcher, B. Whittle, R. Chand, N. Fewings, M. Field, D. Andrews, C.C. Goodnow, and M.C. Cook. 2014. Autosomal-dominant B-cell deficiency with alopecia due to a mutation in NFKB2 that results in nonprocessable p100. *Blood*. 124:2964–2972. http://dx.doi.org/10.1182/blood-2014-06-578542

Li, H., and R. Durbin. 2009. Fast and accurate short read alignment with Burrows-Wheeler transform. *Bioinformatics*. 25:1754–1760. http://dx.doi.org/10.1093/bioinformatics/btp324

Li, H., B. Handsaker, A. Wysoker, T. Fennell, J. Ruan, N. Homer, G. Marth, G. Abecasis, and R. Durbin. 1000 Genome Project Data Processing Subgroup. 2009. The Sequence Alignment/Map format and SAMtools. *Bioinformatics*. 25:2078–2079. http://dx.doi.org/10.1093/bioinformatics/btp352

Liang, Y., R.E. Seymour, and J.P. Sundberg. 2011. Inhibition of NF-κB signaling retards eosinophilic dermatitis in SHARPIN-deficient mice. *J. Invest. Dermatol.* 131:141–149. http://dx.doi.org/10.1038/jid.2010.259

Lindsley, A.W., Y. Qian, C.A. Valencia, K. Shah, K. Zhang, and A. Assa'ad. 2014. Combined immune deficiency in a patient with a novel NFKB2 mutation. *J. Clin. Immunol.* 34:910–915. http://dx.doi.org/10.1007/s10875-014-0095-3

MacDuff, D.A., T.A. Reese, J.M. Kimmey, L.A. Weiss, C. Song, X. Zhang, A. Kambal, E. Duan, J.A. Carrero, B. Boisson, et al. 2015. Phenotypic complementation of genetic immunodeficiency by chronic herpesvirus infection. *eLife*. 4:e04494. http://dx.doi.org/10.7554/eLife.04494

Matsumoto, M.L., K.C. Dong, C. Yu, L. Phu, X. Gao, R.N. Hannoush, S.G. Hymowitz, D.S. Kirkpatrick, V.M. Dixit, and R.F. Kelley. 2012. Engineering and structural characterization of a linear polyubiquitin-specific antibody. *J. Mol. Biol.* 418:134–144.

McKenna, A., M. Hanna, E. Banks, A. Sivachenko, K. Cibulskis, A. Kernytsky, K. Garimella, D. Altshuler, S. Gabriel, M. Daly, and M.A. DePristo. 2010. The Genome Analysis Toolkit: a MapReduce framework for analyzing next-generation DNA sequencing data. *Genome Res.* 20:1297–1303. http://dx.doi.org/10.1101/gr.107524.110

Mousallem, T., J. Yang, T.J. Urban, H. Wang, M. Adeli, R.E. Parrott, J.L. Roberts, D.B. Goldstein, R.H. Buckley, and X.P. Zhong. 2014. A nonsense mutation in IKBKB causes combined immunodeficiency. *Blood*. 124:2046–2050. http://dx.doi.org/10.1182/blood-2014-04-571265

Nielsen, C., M.A. Jakobsen, M.J. Larsen, A.C. Müller, S. Hansen, S.T. Lillevang, N. Fisker, and T. Barington. 2014. Immunodeficiency associated with a nonsense mutation of IKBKB. *J. Clin. Immunol.* 34:916–921. http://dx.doi.org/10.1007/s10875-014-0097-1

Nilsson, J., B. Schoser, P. Laforet, O. Kalev, C. Lindberg, N.B. Romero, M. Dávila López, H.O. Akman, K. Wahbi, S. Iglseder, et al. 2013. Polyglucosan body myopathy caused by defective ubiquitin ligase RBCK1. *Ann. Neurol.* 74:914–919. http://dx.doi.org/10.1002/ana.23963

Pannicke, U., B. Baumann, S. Fuchs, P. Henneke, A. Rensing-Ehl, M. Rizzi, A. Janda, K. Hese, M. Schlesier, K. Holzmann, et al. 2013. Deficiency of innate and acquired immunity caused by an IKBKB mutation. *N. Engl. J. Med.* 369:2504–2514. http://dx.doi.org/10.1056/NEJMoa1309199

Peltzer, N., E. Rieser, L. Taraborrelli, P. Draber, M. Darding, B. Pernaute, Y. Shimizu, A. Sarr, H. Draberova, A. Montinaro, et al. 2014. HOIP deficiency causes embryonic lethality by aberrant TNFR1-mediated endothelial cell death. *Cell Reports*. 9:153–165. http://dx.doi.org/10.1016/j.celrep.2014.08.066

Picard, C., A. Puel, M. Bonnet, C.L. Ku, J. Bustamante, K. Yang, C. Soudais, S. Dupuis, J. Feinberg, C. Fieschi, et al. 2003. Pyogenic bacterial infections in humans with IRAK-4 deficiency. *Science*. 299:2076–2079. http://dx.doi.org/10.1126/science.1081902

Picard, C., H. von Bernuth, P. Ghandil, M. Chrabieh, O. Levy, P.D. Arkwright, D. McDonald, R.S. Geha, H. Takada, J.C. Krause, et al. 2010. Clinical features and outcome of patients with IRAK-4 and MyD88 deficiency. *Medicine (Baltimore)*. 89:403–425. http://dx.doi.org/10.1097/MD.0b013e3181fd8ec3

Picard, C., J.L. Casanova, and A. Puel. 2011. Infectious diseases in patients with IRAK-4, MyD88, NEMO, or IκBα deficiency. *Clin. Microbiol. Rev.* 24:490–497. http://dx.doi.org/10.1128/CMR.00001-11

Popovic, D., D. Vucic, and I. Dikic. 2014. Ubiquitination in disease pathogenesis and treatment. *Nat. Med.* 20:1242–1253. http://dx.doi.org/10.1038/nm.3739

Puel, A., C. Picard, C.L. Ku, A. Smahi, and J.L. Casanova. 2004. Inherited disorders of NF-kappaB-mediated immunity in man. *Curr. Opin. Immunol.* 16:34–41. http://dx.doi.org/10.1016/j.coi.2003.11.013

Recher, M., L.J. Berglund, D.T. Avery, M.J. Cowan, A.R. Gennery, J. Smart, J. Peake, M. Wong, S.Y. Pai, S. Baxi, et al. 2011. IL-21 is the primary common γ chain-binding cytokine required for human B-cell differentiation in vivo. *Blood*. 118:6824–6835. http://dx.doi.org/10.1182/blood-2011-06-362533

Rodgers, M.A., J.W. Bowman, H. Fujita, N. Orazio, M. Shi, Q. Liang, R. Amatya, T.J. Kelly, K. Iwai, J. Ting, and J.U. Jung. 2014. The linear ubiquitin assembly complex (LUBAC) is essential for NLRP3 inflammasome activation. *J. Exp. Med.* 211:1333–1347. http://dx.doi.org/10.1084/jem.20132486

Sasaki, Y., S. Sano, M. Nakahara, S. Murata, K. Kometani, Y. Aiba, S. Sakamoto, Y. Watanabe, K. Tanaka, T. Kurosaki, and K. Iwai. 2013. Defective immune responses in mice lacking LUBAC-mediated linear ubiquitination in B cells. *EMBO J.* 32:2463–2476. http://dx.doi.org/10.1038/emboj.2013.184

Schaeffer, V., M. Akutsu, M.H. Olma, L.C. Gomes, M. Kawasaki, and I. Dikic. 2014. Binding of OTULIN to the PUB domain of HOIP controls NF-κB signaling. *Mol. Cell.* 54:349–361. http://dx.doi.org/10.1016/j.molcel.2014.03.016

Seymour, R.E., M.G. Hasham, G.A. Cox, L.D. Shultz, H. Hogenesch, D.C. Roopenian, and J.P. Sundberg. 2007. Spontaneous mutations in the mouse Sharpin gene result in multiorgan inflammation, immune system dysregulation and dermatitis. *Genes Immun.* 8:416–421. http://dx.doi.org/10.1038/sj.gene.6364403

Smahi, A., G. Courtois, P. Vabres, S. Yamaoka, S. Heuertz, A. Munnich, A. Israël, N.S. Heiss, S.M. Klauck, P. Kioschis, et al. The International Incontinentia Pigmenti (IP) Consortium. 2000. Genomic rearrangement in NEMO impairs NF-kappaB activation and is a cause of incontinentia pigmenti. *Nature*. 405:466–472. http://dx.doi.org/10.1038/35013114

Smit, J.J., D. Monteferrario, S.M. Noordermeer, W.J. van Dijk, B.A. van der Reijden, and T.K. Sixma. 2012. The E3 ligase HOIP specifies linear ubiquitin chain assembly through its RING-IBR-RING domain and the unique LDD extension. *EMBO J.* 31:3833–3844. http://dx.doi.org/10.1038/emboj.2012.217

Stieglitz, B., R.R. Rana, M.G. Koliopoulos, A.C. Morris-Davies, V. Schaeffer, E. Christodoulou, S. Howell, N.R. Brown, I. Dikic, and K. Rittinger. 2013. Structural basis for ligase-specific conjugation of linear ubiquitin chains by HOIP. *Nature*. 503:422–426. http://dx.doi.org/10.1038/nature12638

Tarantino, N., J.Y. Tinevez, E.F. Crowell, B. Boisson, R. Henriques, M. Mhlanga, F. Agou, A. Israël, and E. Laplantine. 2014. TNF and IL-1 exhibit distinct ubiquitin requirements for inducing NEMO-IKK supramolecular structures. *J. Cell Biol.* 204:231–245. http://dx.doi.org/10.1083/jcb.201307172

Tokunaga, F., S. Sakata, Y. Saeki, Y. Satomi, T. Kirisako, K. Kamei, T. Nakagawa, M. Kato, S. Murata, S. Yamaoka, et al. 2009. Involvement of linear polyubiquitylation of NEMO in NF-kappaB activation. *Nat. Cell Biol.* 11:123–132. http://dx.doi.org/10.1038/ncb1821

Tokunaga, F., T. Nakagawa, M. Nakahara, Y. Saeki, M. Taniguchi, S. Sakata, K. Tanaka, H. Nakano, and K. Iwai. 2011. SHARPIN is a component of the NF-κB-activating linear ubiquitin chain assembly complex. *Nature*. 471:633–636. http://dx.doi.org/10.1038/nature09815

von Bernuth, H., C. Picard, Z. Jin, R. Pankla, H. Xiao, C.L. Ku, M. Chrabieh, I.B. Mustapha, P. Ghandil, Y. Camcioglu, et al. 2008. Pyogenic bacterial infections in humans with MyD88 deficiency. *Science*. 321:691–696. http://dx.doi.org/10.1126/science.1158298

Wang, K., C. Kim, J. Bradfield, Y. Guo, E. Toskala, F.G. Otieno, C. Hou, K. Thomas, C. Cardinale, G.J. Lyon, et al. 2013. Whole-genome DNA/RNA sequencing identifies truncating mutations in RBCK1 in a novel Mendelian disease with neuromuscular and cardiac involvement. *Genome Med.* 5:67. http://dx.doi.org/10.1186/gm471

Willmann, K.L., S. Klaver, F. Doğu, E. Santos-Valente, W. Garncarz, I. Bilic, E. Mace, E. Salzer, C.D. Conde, H. Sic, et al. 2014. Biallelic loss-of-function mutation in NIK causes a primary immunodeficiency with multifaceted aberrant lymphoid immunity. *Nat. Commun.* 5:5360. http://dx.doi.org/10.1038/ncomms6360

Zak, D.E., F. Schmitz, E.S. Gold, A.H. Diercks, J.J. Peschon, J.S. Valvo, A. Niemistö, I. Podolsky, S.G. Fallen, R. Suen, et al. 2011. Systems analysis identifies an essential role for SHANK-associated RH domain-interacting protein (SHARPIN) in macrophage Toll-like receptor 2 (TLR2) responses. *Proc. Natl. Acad. Sci. USA*. 108:11536–11541. http://dx.doi.org/10.1073/pnas.1107577108